The Journal of Experimental Biology 210, 2548-2562
Published by The Company of Biologists 2007
doi:10.1242/jeb.02792

Running in ostriches (*Struthio camelus*): three-dimensional joint axes alignment and joint kinematics

Jonas Rubenson[1,*], David G. Lloyd[1], Thor F. Besier[2], Denham B. Heliams[3] and Paul A. Fournier[1]

[1]*School of Human Movement and Exercise Science, The University of Western Australia, Crawley, WA, 6009, Australia,* [2]*Department of Orthopaedics, Stanford University, 341 Galvez St, Stanford, CA 94305, USA and* [3]*Fauna Technology, PO Box 558, Gosnells, WA, 6990, Australia*

*Author for correspondence (e-mail: jrubenson@csupomona.edu)

Accepted 16 May 2007

Summary

Although locomotor kinematics in walking and running birds have been examined in studies exploring many biological aspects of bipedalism, these studies have been largely limited to two-dimensional analyses. Incorporating a five-segment, 17 degree-of-freedom (d.f.) kinematic model of the ostrich hind limb developed from anatomical specimens, we quantified the three-dimensional (3-D) joint axis alignment and joint kinematics during running (at ~3.3 m s^{-1}) in the largest avian biped, the ostrich. Our analysis revealed that the majority of the segment motion during running in the ostrich occurs in flexion/extension. Importantly, however, the alignment of the average flexion/extension helical axes of the knee and ankle are rotated externally to the direction of travel (37° and 21°, respectively) so that pure flexion and extension at the knee will act to adduct and adbuct the tibiotarsus relative to the plane of movement, and pure flexion and extension at the ankle will act to abduct and adduct the tarsometatarsus relative to the plane of movement. This feature of the limb anatomy appears to provide the major lateral (non-sagittal) displacement of the lower limb necessary for steering the swinging limb clear of the stance limb and replaces what would otherwise require greater adduction/abduction and/or internal/external rotation, allowing for less complex joints, musculoskeletal geometry and neuromuscular control. Significant rotation about the joints' non-flexion/extension axes nevertheless occurs over the running stride. In particular, hip abduction and knee internal/external and varus/valgus motion may further facilitate limb clearance during the swing phase, and substantial non-flexion/extension movement at the knee is also observed during stance. Measurement of 3-D segment and joint motion in birds will be aided by the use of functionally determined axes of rotation rather than assumed axes, proving important when interpreting the biomechanics and motor control of avian bipedalism.

Key words: kinematics, ostrich, bird, three-dimensional, locomotion, joint.

Introduction

The vast majority of bipedal species are birds, which are thus valuable for understanding the biology of bipedal locomotion. Hind limb kinematics of terrestrial locomotion in birds has been used to study locomotor behavior (Reilly, 2000; Verstappen et al., 2000), muscle function (Clark and Alexander, 1975; Roberts and Scales, 2004), neural and motor control (Johnston and Bekoff, 1992; Johnston and Bekoff, 1996; Verstappen and Aerts, 2000), ontogeny of locomotion (Muir et al., 1996) and locomotor energetics (Fedak et al., 1982; Roberts et al., 1998; Roberts and Scales, 2004; Rubenson et al., 2004). Hind-limb kinematics of birds has also been used to explore the evolution of avian bipedalism and archosaur locomotion in general (Gatesy and Biewener, 1991; Gatesy, 1999; Hutchinson and Gatesy, 2000), and has been used to aid predictions of the locomotor abilities of extinct bipedal taxa (Hutchinson, 2004).

A significant limitation of past kinematic studies, however, is the general reliance on two-dimensional (2-D) planar analyses. Analyses in 2-D have been found to be insufficient for understanding the movement of many terrestrial species. This is particularly apparent in those animals with sprawled postures, whose limb segments are not aligned in the sagittal plane [e.g. lizards and crocodylians (Gatesy, 1991; Reilly and Elias, 1998; Irschick and Jayne, 1999; Jayne and Irschick, 1999]. The importance of incorporating three-dimensional (3-D) kinematics is not restricted to sprawling gaits. Indeed, 3-D kinematics are necessary for revealing fundamental aspects of human locomotion, many of which have direct clinical application (Whittle, 1995), and some studies indicate that 3-D limb motions also occur in running birds (Cracraft, 1971; Gatesy, 1999), although no comprehensive joint analyses during locomotion have been undertaken.

Examination of human kinematics has revealed that not only limb posture, but also the alignment of the joint axes, play an important role in determining the 3-D nature of limb movements (Piazza and Cavanagh, 2000; Besier et al., 2003; Most et al., 2004). Indeed, Piazza and Cavanagh (Piazza and Cavanagh, 2000) illustrated that a small misalignment between the assumed

joint axes of rotation and the true axis about which rotation occurs can result in considerable kinematic cross-talk [when one joint rotation (e.g. adduction) is interpreted as another (e.g. flexion)].

Avian bipeds possess a relatively upright hind-limb posture, aligned primarily in the sagittal plane. Birds have substantial limb displacement in the frontal plane compared to humans, however, owing primarily to a more abducted femur. The combined effect of limb posture and joint axes alignment may result in significant 3-D hind-limb motion in birds that may hold important information regarding the mechanics and neuromuscular control of bipedal locomotion and its evolution (Hutchinson and Gatesy, 2000; Biewener, 2002).

In this paper we present full 3-D joint kinematic data of running in the largest avian biped, the ostrich (*Struthio camelus*). Ostriches were chosen because they are of comparable size to humans, thus facilitating the use of established 3-D gait techniques, and furthermore, because they allow comparisons between avian and human 3-D kinematics without the confounding effect of body mass. A comparison between humans and ostriches thus provides a unique opportunity to reveal general features of bipedal locomotion and those unique to human and avian bipeds (the two extant representatives of obligate bipedalism) that arise specifically from differences in limb structure.

The first aim of this paper was the development of a 3-D joint kinematic model of the ostrich hind limb from anatomical specimens. This model uses mathematically determined functional joint axes and centers of rotation to describe joint axis alignment and motion. The second aim involved incorporating this kinematic model to investigate the 3-D joint angles of the ostrich during running.

Materials and methods

Animals

Fresh hind limbs from two healthy specimens of *Struthio camelus* L. (body mass 71.7 kg and 85.0 kg), obtained from a local farm and a local abattoir, were used for anatomical joint kinematic modeling. Five ostriches obtained from a local breeder were hand-reared and trained for over-ground running. However, only two animals (mass 70.0 kg and 78.7 kg) were amenable to the procedures required for full 3-D joint kinematic analysis. A third animal (mass 75.9 kg) provided additional data on 3-D pelvic motion as well as overall 3-D limb displacement, which matched closely those of the other two individuals. Animals were kept in a large outdoor field (5000 m^2) and provided with unlimited access to food and water. All experiments were performed in accordance with the Animal Ethics Committee of the University of Western Australia.

Model development

A five-segment, 17 degree-of-freedom (d.f.) kinematic model of the ostrich hind limb was developed from anatomical specimens that can be reconstructed on living animals using only 3-D anatomical landmark (AL) data. This model included the pelvis/trunk, femur, tibiotarsus, tarsometatarsus and phalanges segments, each modeled as a rigid body. The position and orientation of each rigid segment in space was defined using segment-embedded anatomical coordinate systems (ACSs) that reflect functionally relevant joint centers and joint axes of rotation (Cappozzo et al., 1995), and were used to describe 3-D joint motion.

The kinematic modeling involved three primary steps. First, anatomical coordinate systems were initially constructed on anatomical specimens because these could not readily be constructed from anatomical landmarks that are palpable on the living animal for several segments of the ostrich hind limb. This involved determining joint centers and functional joint axes of rotation using both dynamic trials (with the exception of the hip), whereby the limb segments were moved through their range of motion, and static trials for the collection of anatomical landmark data (see Table A1 in Appendix for AL definitions). This procedure also provided a basis for comparing the unloaded (passive) joint axes to those measured during running. Secondly, the computed anatomical coordinate systems from the anatomical specimen were expressed in a coordinate system that could be constructed on the live animal using palpable and projected anatomical landmarks (referred to here as technical anatomical coordinate systems, or TACSs). Finally, segment dimensions from the anatomical specimens were collected using anatomical landmarks that were easy to locate on the live animals, allowing scaling factors to be applied to the reconstruction of the anatomical coordinate systems on the live animals.

Static 3-D anatomical data and 3-D segment motion were collected using a six-camera VICON motion analysis system (Oxford Metrics, Oxford, UK). Cameras were strategically placed around the limb to minimize marker occlusion and maximize marker resolution. The intact limb, including the pelvis was positioned on a steel mesh stage that enabled each segment to be either fixed securely or to be moved through its range of motion. Three stainless steel self-tapping screws were placed into the femur, tibiotarsus, tarsometatarsus and phalanges in a non-collinear configuration onto which retro-reflective markers (20 mm) were placed. The placement of the screws required only minimal dissection of surrounding muscle tissue. The markers were used to construct rigid-body technical coordinate systems (TCSs) for these segments during both static and dynamic trials.

For static trials, anatomical landmarks were located using a five-marker pointer. Marker redundancy was used to reduce the error in locating the end of the pointer. During dynamic trials, the proximal segment was secured to the mesh stage whilst the distal segment was moved through its range of motion. Motion data of the markers was collected at 50 Hz with a resolution better than 2 mm. Segment motion was allowed to follow the natural path of the joint, and because the weight of the limbs could affect the joint posture, the dynamic trials were made with the stage positioned upright.

The functional flexion/extension axis of the knee, ankle and metatrso-phalangeal joints were derived from motion data of the distal segment with respect to the proximal segment. To achieve this, three cycles of flexion/extension over the joints full range of motion were captured. Using a custom-written MATLAB program (Mathworks Inc., Natick, MA, USA) the motion data were filtered (fourth order zero-lag Butterworth low-pass filter) and the distal markers expressed relative to the proximal technical coordinate system. Instantaneous finite helical axes were calculated throughout the range of motion using the

singular value decomposition method [(Spoor and Veldpaus, 1980; Reinschmidt and van den Bogert, 1997); any 3-D rigid body motion can be explained by a rotation about, and translation along, an axis known as the helical (or screw) axis]. A mean helical axis was calculated for the joint relative to the proximal segment's technical coordinate system and was used to define the functional flexion/extension axis of the joint as per Besier et al. (Besier et al., 2003). The medial and lateral borders of the knee, ankle and metatarso-phalangeal joints were then expressed relative to the proximal segment's technical coordinate system, thereby creating a vector that described the width of the joint. The knee, ankle and metatarso-phalangeal joint centers were subsequently defined as the average of two points on the mean helical axis, these being: (1) the intersection of the mean helical axis with a plane that was normal to the mean helical axis that went through the midpoint of the vector describing the width of the joint, and (2) the intersection of the mean helical axis with a plane normal to the vector describing the width of the joint and going through the midpoint of the this vector (Fig. 1).

Although the hip joint center has been located on humans using numerical optimization of motion data of the thigh (Cappozzo, 1984; Leardini et al., 1999), this is not feasible for ostriches since the femur has a very small range of motion (Gatesy and Biewener, 1991), which can result in error (Piazza et al., 2004). Instead, the hip joint center was defined statically. After disarticulating the femur from the pelvis, the center of the head of the femur (assumed to be the joint center) was identified relative to the femur technical coordinate system. This was done by bisecting a vector defined by two points on opposite sides of the head of the femur, which was assumed to represent the diameter of the head of the femur.

The segment anatomical coordinate systems for the femur, tibiotarsus, tarsometatarsus and phalanges were defined using the calculated joint centers and mean flexion/extension helical axes. The pelvis/trunk ACS was defined using the following anatomical landmarks: (1) the cranial aspect of the ilium, where it meets the sixth thoracic vertebrae (IL), (2) the caudal end of the prominent ridge on the midline of the dorsal aspect of the postacetabular ilium (SUL) and (3) the caudal end of the synsacrum where it meets the first tail vertebra (SYN). See the Appendix for details of the definition of the segment ACSs and Fig. 2 for a graphical representation of the segment ACSs.

To re-construct the anatomical coordinate systems on the live animal, TACSs were defined on the anatomical specimen using a combination of palpable anatomical landmarks on the live animal and numerically derived landmarks based on these ALs. See the Appendix for a list of anatomical and derived landmarks and for detailed description of TACS definitions. The points used in each of the segment's anatomical coordinate system were then expressed relative to their TACSs, allowing the ACS to be constructed. In order to accommodate for slight differences in limb dimension between the anatomical specimens and the experimental animals, scaling factors were used to scale the location of the ACS points in the TACSs. This scaling assumed linear proportionality between the live animals and the anatomical specimens. The scaling factors used for each TACS are listed in the Appendix (Table A2) and the location of the ACS points are presented as a percent of the scale distances. Where more than one scaling factor is presented for a given point, the location of the point on the experimental animal was taken as the average of the two projected points.

Hip, knee, ankle and metatarso-phalangeal joint angle motions on the live animals were computed using the kinematic model (constructed from the laboratory limb segments) in BodyBuilder software (Oxford Metrics, Oxford, UK). For comparison, knee and ankle joint angles were also computed from the motion of the anatomical limb specimens in the laboratory trials. This was achieved by re-constructing each segment's ACS using the optimized joint flexion/extension axes and joint centers, as outlined above and in the Appendix. The ACSs of the proximal and distal segments at each joint were used to define the joint coordinate system, the set of three ordered joint angle rotations as per the ISB standard (Grood and Suntay, 1983; Wu and Cavanagh, 1995). The first rotation was about the *z*-axis of the proximal segment's ACS (the flexion/extension rotation; positive rotation represented flexion and negative rotation represented extension). The last rotation was about the *y*-axis of the distal segment's ACS (the long-axis rotation; positive rotation represented internal rotation and negative rotation represented external rotation). The middle rotation was about a floating axis, which is perpendicular to first and last rotation axes (the abduction/adduction rotation; positive rotation represented adduction and negative rotation represented abduction). The zero joint angles occur when the segments' ACSs lie in a straight line, except for the metatarso-phalangeal joint, where zero flexion/extension occurs when the phalanges and tarsometatarsus are perpendicular to one another, akin to the human ankle. It should be noted that the joint coordinate system is generally non-orthogonal.

On the live animals, pelvic segment angles were defined by the rotation of the pelvis ACS relative to the global coordinate system. Pelvic pitch was defined as the rotation about the *z*-axis of the segment, where a positive angle represents an upward pitch. Roll was defined as the rotation about the *x*-axis of the segment, where a positive angle represents a lateral (long-axis) rotation to the right. Yaw was defined as the rotation about the *y*-axis of the moving frame, where a negative angle represents an external rotation of the segment relative to the direction of travel (a rotation to the right).

Running kinematics

A 50-m long and 2-m wide fenced runway was constructed within the animal's field. The runway was surfaced with high-density rubber matting (10 mm thickness). Within a large enclosure, two 200 Hz synchronized high-speed video cameras (Peak Performance; Centenial, CO, USA) were placed at a 45° angle to the track. In order to provide suitable lighting for night trials, 2000 W floodlighting was used behind each camera. A weatherproof tent housed the video data acquisition system.

An 11-parameter, 83 d.f. direct linear transformation (DLT) was used to construct a ~3 m^3 calibration volume from the two camera views using Peak Motus software (Peak Performance; Centenial, CO, USA). The DLT was calculated using a custom-built 48-point moveable calibration frame. The average mean square error in the *x*-, *y*- and *z*-directions from the DLT was 6.0, 3.0 and 5.0 mm, respectively, and the average percent volume error was 0.19%. The video cameras were manually switched

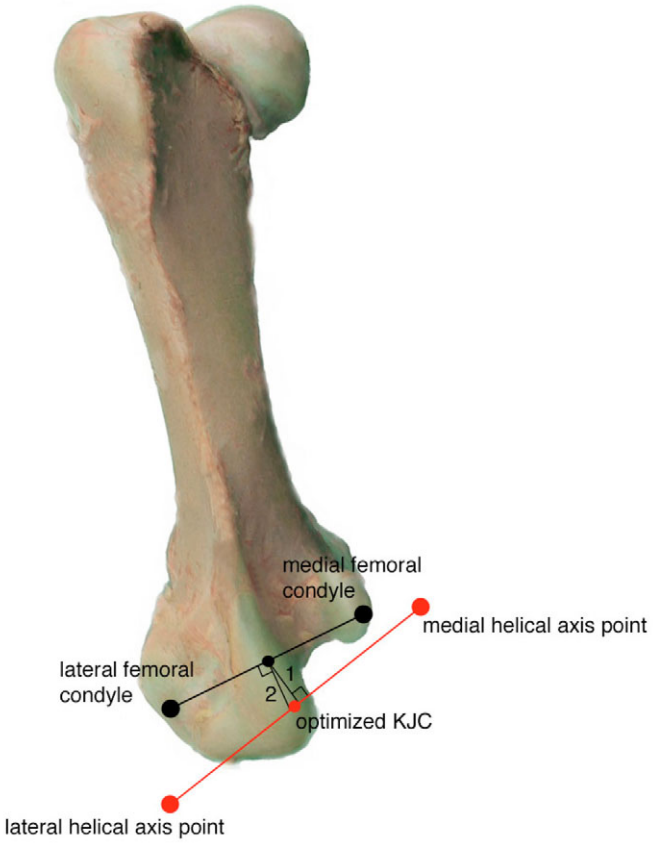

Fig. 1. A graphical representation of the optimized right knee joint center (KJC) observed from an anterior aspect. Planes 1 and 2 are defined by a point on the helical axis and the midpoint of the transepicondylar vector. The KJC is the average of the points on the helical axis intersected by planes 1 and 2. The distance between the transepicondylar vector and the helical axis in this figure is not to scale.

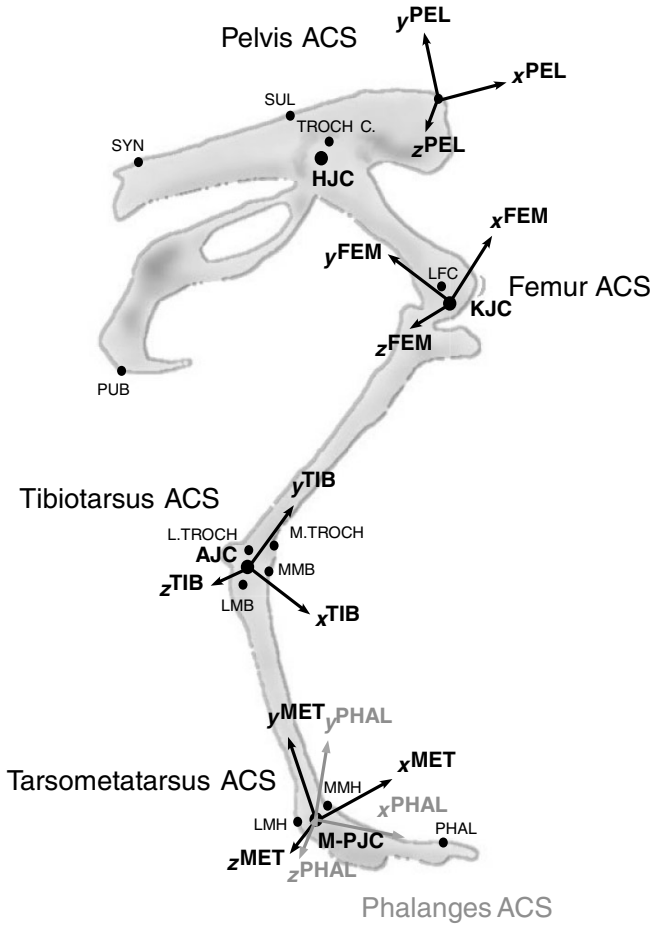

Fig. 2. Anatomical Coordinate Systems (ACS) of the hind-limb model and location of anatomical landmarks (AL). Figure produced from bone tracings (Immersion InScribe3) using MATLAB software (Mathworks, Natick, MA). PUB (caudal end of pubis) is an alternative point for the construction of a pelvis ACS. The location of the joint centers and anatomical landmarks do not represent exact locations in this figure. PEL, pelvis; FEM, femur; TIB, tibiotarsus, MET, tarsometatarsus; PHAL, phalanges; for other abbreviations, see Table A1.

on when the birds were viewed (on real-time monitors) commencing their run. The animal's instantaneous running velocity was determined from the pelvis origin throughout the calibrated volume. In order to help determine if the animal was running at a steady speed before entering and after exiting the calibrated volume, we used either visual markers that were spatially calibrated in the horizontal direction only, or electronic timing gates, from which running velocity was calculated over a 10 m distance either side of the center of the calibrated volume. All data collections were performed after sunset under artificial lighting, which permitted the use of retro-reflective markers that improved marker location and also avoided high ambient day temperatures. Performing trials at night also meant that the birds were, in general, more amenable to experimentation than in daylight hours.

To determine the 3-D position and orientation of each segment during each running trial, clusters of retro-reflective markers (20 mm) were used to define TCSs. Marker clusters were attached to the pelvis, femur, tibiotarsus and tarsometatarsus, and a single marker was attached to the third phalanx of digit III (Fig. 3). In order to secure these markers to the animal and to ensure that they were visible during testing, the feathers surrounding the marker placements were removed and some wing feathers were clipped. The pelvis markers consisted of wands that were fit with two in-line markers. These wands were placed directly over the IL, SUL and SYN (Figs 2 and 3). The wand markers were attached to a rubber base and secured to the bird using double-sided tape. The femur cluster consisted of three non-co-linear markers mounted on a high-density foam base and secured to the skin using double-sided tape. For the tibiotarsus and tarsometatarsus, rubber cuffs containing four non-co-planar markers were fastened around the limb using double sided-tape and further secured using tape on the outside of the cuff.

Static calibration trials were used to locate the anatomical landmarks required to re-construct the segment anatomical coordinate systems. The animals were positioned in the center of the calibration volume and, with the exception of the pelvis, the anatomical landmarks were located using a six-marker pointer device similar to that used in the anatomical modeling

and expressed relative to the respective TCS (Fig. 3). The pelvis anatomical landmarks were located directly from the in-line wand markers by projecting a known distance from the bottom marker along the vector defined by the two in-line markers. Since the wands pivoted about their respective anatomical landmarks, this system of defining the pelvis/trunk TCS had the advantage of not being greatly affected by marker movement.

The motion data of the limb marker clusters from the running trials also allowed for a direct calculation of optimized helical flexion/extension axes for the knee and ankle. The computed helical axes from the running trials were compared to those reconstructed from the kinematic model *via* static calibration trials.

Marker locations in the video footage were digitized using PEAK Motus software. The *x*-, *y*- and *z*-component of each marker trajectory was filtered using a fourth order zero-lag Butterworth low-pass filter. The filter cut-off frequency was set to within the range 4–12 Hz upon visual inspection of the filtered *versus* unfiltered data. The video data were appended to a single C3d 'REAL' data file using C3d-Editor software (Motion Lab Systems, USA). From these files, the 3-D joint kinematics were computed using BodyBuilder modeling software, as described above.

Statistics

Six trials per animal were computed. Gait data were normalized to 100 points over one stride using a cubic spline interpolation to facilitate compilation of multiple trials so that the mean ± standard deviation (s.d.) of the kinematic curves could be determined.

Results

Anatomical specimen joint kinematics

Motion of the anatomical limb segments showed that both the knee and ankle joints exhibited considerable passive motion about their adduction/abduction axis and longitudinal axis that were coupled with flexion/extension (Fig. 4). Flexion at the knee was coupled to valgus and external rotation motion. A 40° increase in knee flexion resulted in ~3° valgus rotation and 4° external rotation. Flexion at the ankle was coupled to adduction and internal rotation motion. A 70° increase in ankle flexion results in ~5° adduction and 3° internal rotation. It should be noted that the passive motion of the knee joint was greatly affected when muscles surrounding the joint were dissected. In trials where muscles crossing the knee had been removed the joint exhibited substantially more non-flexion/extension movement and with a different pattern to that when the musculature was left intact. For this reason, only trials where the musculature surrounding the knee was kept intact were used in the model construction.

Joint axes orientation

Reconstruction of the kinematic model on live animals revealed substantial rotation of the joint axes of rotation relative to the plane of movement (Fig. 5). The knee's flexion/extension axis had a mean external rotation angle of 37° relative to the sagittal plane (the plane defined by the global coordinate system *x*- and *z*-axis unit vectors) across the running stride. A minimum rotation of 31° occurred just prior to mid-swing and a maximum rotation of 42° occurred just prior to toe-strike. The flexion/extension axis of the ankle had a mean external rotation angle of 21° relative to the sagittal plane across the running stride. The ankle flexion/extension axis exhibited a maximum external rotation of 33° prior to toe-strike and a minimum rotation of 9° at mid-swing. The metatarso-phalangeal joint exhibited a mean external rotation angle of 26° relative to the sagittal plane across the running stride.

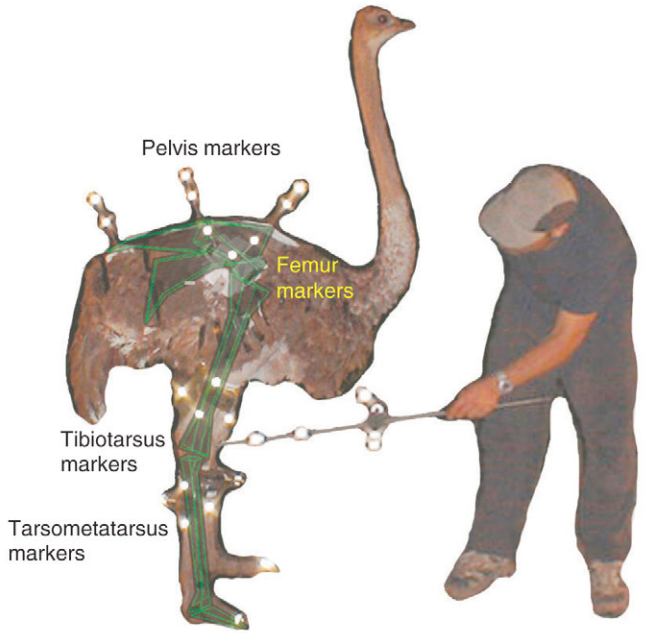

Fig. 3. Segment marker clusters used to construct the segment technical coordinate systems (TCSs) and the pointing device used for identifying anatomical landmarks (ALs) required for reconstructing the kinematic model.

Running spatio-temporal kinematics

When prompted to run, the birds selected a relatively narrow range of speeds (~2.5–4.0 m s^{-1}), although some faster and slower speeds were observed outside this range. The subset of strides used for analysis in this study (3.29±0.30 m s^{-1}; mean ± s.d.) were chosen on the basis of their closeness in speed and whether they maintained their running speed through the calibrated volume. The animals' naturally chosen running speed was ~3.3 m s^{-1} during our experiments and, although much slower than their maximum running speed, this speed is biomechanically and energetically representative of running in this species (Rubenson et al., 2004). Nevertheless, it is not certain whether the joint kinematic patterns are necessarily the same at much faster running speeds. The animals ran with a stride length of 2.32±0.25 m (mean ± s.d.) and a stride frequency of 1.42±0.05 Hz (mean ± s.d.). Time of contact and limb-swing time (of individual limbs) were 0.30±0.02 s and 0.40±0.04 s (mean ± s.d.), respectively, resulting in a duty factor of 0.43±0.04 (mean ± s.d.).

Running segmental and joint kinematics

Pelvic roll exhibited small excursions, with an inconsistent pattern over the running stride (Fig. 6A). A pattern whereby the pelvis is rotated internally about its long axis during the early part of the swing and rotated externally at the end of swing may be present, although difficult to discern given the measurement variability. Pelvic pitch had two excursions of up to 6° around a mean angle of 12.5° (Fig. 6B). The pelvic pitch peaked at mid-swing and decreased until it reached a minimum just after toe-strike. The pelvis pitched upwards until a second peak during mid-stance and then decreased until it reached a second minimum shortly after toe-off. The pelvis remained very stable in the yaw direction, fluctuating less than 1° from the neutral position throughout the gait cycle (Fig. 6C).

The hip remained in a flexed posture throughout the stride, with hip flexion/extension fluctuating as much as 12.7° (Fig. 7A). During early swing, the hip joint remains relatively stationary, and then flexes during the later half of swing phase (~10°). After toe-strike, the hip exhibits a brief period of extension followed by flexion (~5°) until reaching a maximum flexion during mid-stance. The second half of the stance phase was characterized by rapid hip extension until toe-off. The pattern of hip adduction/abduction was similar to hip flexion/extension with a marginally smaller joint excursion (9.5°) (Fig. 7B). During the swing phase, the hip was abducted. After toe-strike the hip undergoes a small adduction/abduction movement until a maximum hip abduction is reached during mid-stance. The hip then adducted rapidly during the second half of stance until maximum hip adduction was reached at toe-off. Little internal/external motion existed throughout most of the stride (Fig. 7C). Towards the end of the stance phase and the early part of swing, the hip rotated internally followed by external rotation during the later half of swing, returning to an apparent neutral position by toe-strike.

Over the running stride, the knee joint underwent substantial excursions about all three joint axes (Fig. 8). The majority of the excursion was in flexion/extension (Fig. 8A), most of which occurred during the swing phase. At toe-off, the knee flexed as the leg was lifted off the ground. By mid-swing, the knee reached maximum flexion and thereafter began to extend as the toes were lowered to the ground. After toe-strike, the knee began to flex and continued to do so up until mid-stance. During the latter part of the stance phase, the knee exhibited a brief period of extension. The knee remained in a valgus posture throughout the stride. However, valgus/varus excursions occurred at the knee both during the swing phase (~15°) and during the stance phase (~10°) (Fig. 8B). The varus/valgus joint angle peaked just after toe-strike and reached a minimum during mid-swing. Substantial internal/external rotation (~20°) occurred at the knee throughout the running stride (Fig. 8C). Throughout most of the stance phase the tibia rotated externally relative to the femur. Between toe-off and mid-swing the knee continued to rotate externally, after which the knee rapidly rotated internally up until toe-strike.

The ankle joint underwent large excursions in flexion/extension over the running stride (Fig. 9A), with nearly the entire flexion/extension excursion occurring in the swing phase. After toe-off, the ankle underwent rapid flexion lifting the toes off the ground, reaching maximum flexion at mid-swing. The ankle then rapidly extended between mid-swing and toe-strike.

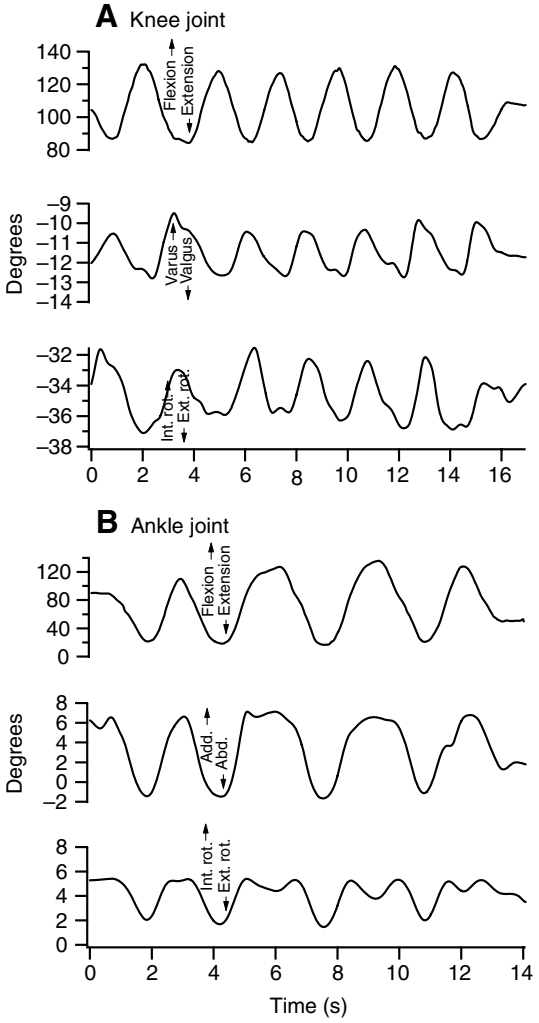

Fig. 4. (A) Knee and (B) ankle joint angles computed from unloaded joint rotation using anatomical specimens. The traces represent a typical pattern of flexion/extension, adduction/abduction (add./abd.; varus/valgus at knee) and internal/external rotation (int. rot./ext. rot.). Both the knee and ankle exhibit coupled internal/external and abduction/adduction (varus/valgus at knee) rotation with passive flexion/extension.

Only a small flexion/extension phase was seen during stance (less than 5°), although moderate joint extension and flexion were observed in the early and late stance phase, respectively. The ankle adduction/abduction joint angle remained relatively constant over the stride (Fig. 9B). A minor adduction/abduction excursion during late swing was observed. During stance the ankle undergoes abduction apart from a small adduction movement prior to toe-off. The ankle exhibited approximately 10° of internal/external rotation over the stride (Fig. 9C). The ankle rotated externally through the stance phase and during the early part of the limb swing followed by internal rotation from mid-swing to toe-strike.

The metatarso-phalangeal joint exhibited the largest flexion/extension excursion of all joints (Fig. 10A), but remained in an extended posture throughout the entire stride. After toe-off the metatarso-phalangeal joint underwent

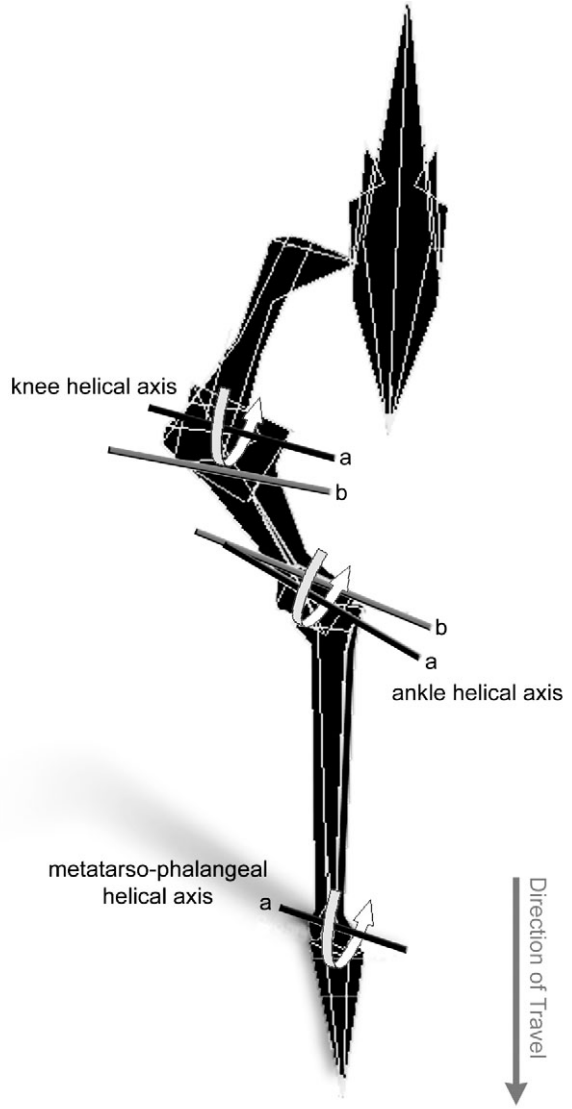

Fig. 5. The orientation of the optimized joint helical axes of the right hind limb viewed from above (prior to toe-strike) using BodyBuilder modeling software (Oxford Metrics; Oxford, UK). a, axes derived from the anatomical specimens; b, axes derived from the running trials.

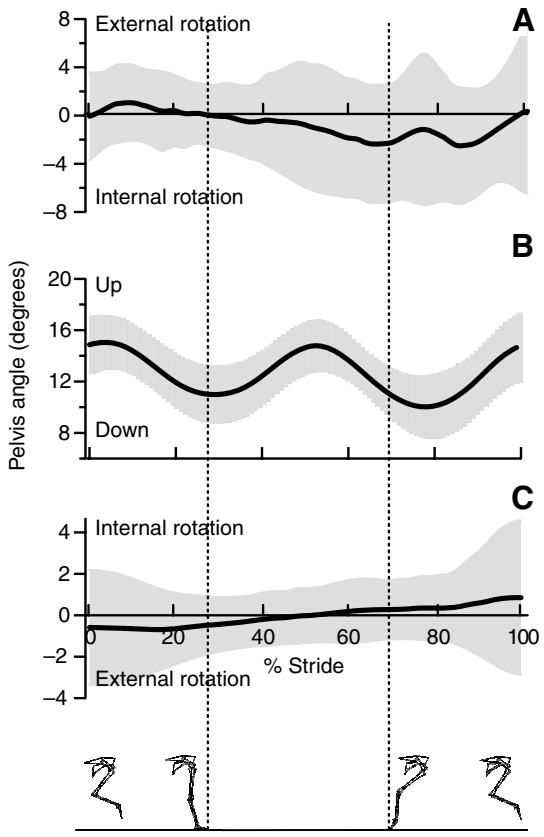

Fig. 6. The pelvis (A) roll, (B) pitch, and (C) yaw angles (relative to the global coordinate system) over one running stride (mean ± s.d.). Each stride begins and ends at mid-swing. The broken lines represent toe-strike and toe-off.

extension, but began to flex prior to mid-swing. The metatarso-phalangeal joint flexed through the remainder of the swing phase and reached a maximum flexion angle at the mid-point of the stance phase. During the second half of the stance phase, the metatarso-phalangeal joint extended. The overall flexion and extension excursions during the stance phase were ~60° and ~80°, respectively. The metatarso-phalangeal joint had little internal/external rotation (toe-in/toe-out) during the majority of stance (Fig. 10B). However, during late stance there was ~5° of rapid external rotation which continued during the early part of the swing phase followed by internal rotation during the latter half of swing.

Discussion

Hind-limb kinematics of terrestrial locomotion in birds has been adopted in studies exploring many biological aspects of bipedalism. The majority of these studies have relied on 2-D sagittal analyses, and the few 3-D interpretations of limb motions are based on anatomical observations or individual planar measurements that are unable to fully explain 3-D motion of the segments and joints. Although these studies are imperative to our understanding of bipedal locomotion, the lack of 3-D data is an important consideration given that much of the information regarding the mechanics and neuromuscular control of bipedal locomotion may reside in the 3-D nature of joint and segment kinematics. Here we show that the hind-limb kinematics of running in the ostrich is characterized by significant non-sagittal segment motion and significant rotation about non-flexion/extension joint axes. Importantly, we reveal that interpretation of 3-D segment and joint motion in the ostrich is aided greatly by the use of functionally determined flexion/extension axes of rotation rather than assumed axes of rotation based on anatomical landmarks.

Comparison to treadmill based ostrich locomotion

Previous kinematic data for ostrich locomotion are sparse and mostly limited to spatio-temporal analyses of animals moving on a treadmill. The subset of strides used for analysis in this study exhibited similar spatio-temporal kinematics to those observed for ostriches running on a motorized treadmill at the same speed (Rubenson et al., 2004). Stride frequency was ~10%

lower in the current study compared to that observed previously (Rubenson et al., 2004), whereas stride length was ~10% greater. Contact time differed little between these studies, but swing time was ~19% longer in over-ground running, which consequently resulted in a 14% difference in duty factor. Much of the differences in stride parameters that exist compared to those previously reported (Rubenson et al., 2004) are likely due to differences in the size of the experimental animals. The birds in the present analysis were slightly larger and therefore expected to possess longer stride lengths and lower stride frequencies. In support of this interpretation, Gatesy and Biewener reported spatio-temporal kinematics from a 90 kg ostrich moving on a treadmill that were similar to those observed in the present study (Gatesy and Biewener, 1991). Nevertheless, the longer strides and slower stride frequency observed in the present study were the result of longer swing times but not longer ground-contact times, possibly the result of differences in treadmill running *versus* over-ground running in ostriches. A study of over-ground locomotion in ratite species (Abourachid and Renous, 2001) indicates that cursorial birds possess longer contact times when moving on a treadmill, resulting in higher duty factors compared to over-ground locomotion at similar speeds.

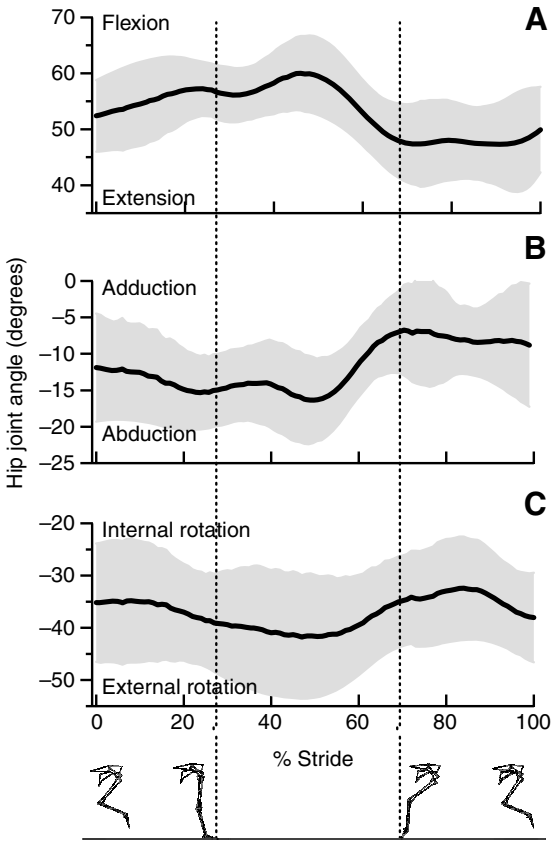

Fig. 7. Hip joint (A) flexion/extension, (B) adduction/abduction and (C) internal/external rotation angles over one running stride (mean ± s.d.). Each stride begins and ends at mid-swing. The broken lines represent toe-strike and toe-off.

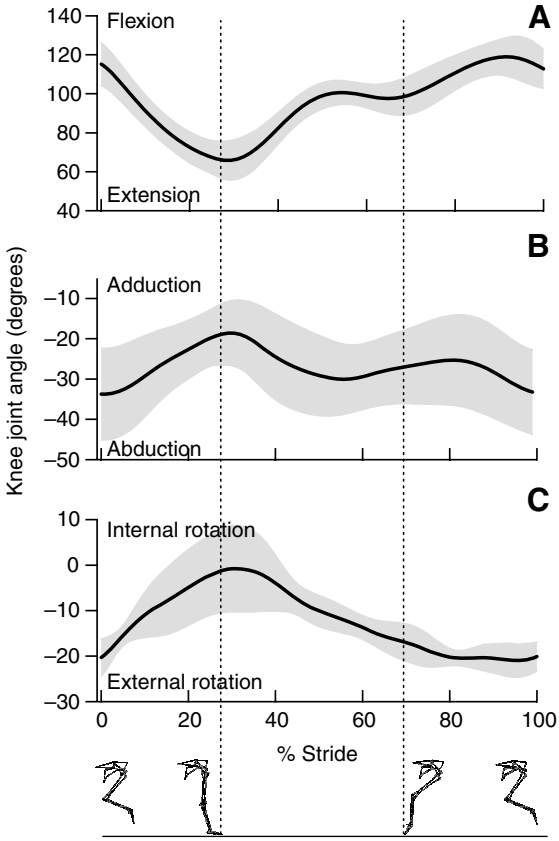

Fig. 8. Knee joint (A) flexion/extension, (B) adduction/abduction and (C) internal/external rotation angles over one running stride (mean ± s.d.). Each stride begins and ends at mid-swing. The broken lines represent toe-strike and toe-off.

Comparison of flexion/extension kinematics to other avian bipeds and humans

The majority of the segment motion during running in the ostrich occurs in flexion/extension, supporting the notion that bipedal locomotion in birds is primarily achieved by sagittal plane movement. In general terms, flexion/extension kinematics in the ostrich is similar to that of other bird species. The small hip excursion in ostriches is consistent with other studies of bird running (e.g. Gatesy and Biewener, 1991; Gatesy, 1999; Reilly, 2000). It is likely, however, that greater hip flexion/extension occurs at faster running speeds. The pattern of hip flexion followed by extension during stance is akin to that observed for running magpies (Verstappen at al., 2000), whereas other avian species such as chickens (Johnston and Bekoff, 1992; Johnston and Bekoff, 1996; Muir et al., 1996), and guinea fowl (Gatesy, 1999) and humans (Novacheck, 1998) exhibit primarily hip extension during stance. It is possible that the flexion–extension countermovement observed at the hip is associated with a stretch–shorten cycle of the muscle–tendon elements and may contribute to storage and release of elastic energy. It is also interesting that, unlike other bird species and humans, ostriches do not exhibit hip extension at the end of the swing phase running at 3.3 m s^{-1}. The knee and ankle joints are therefore

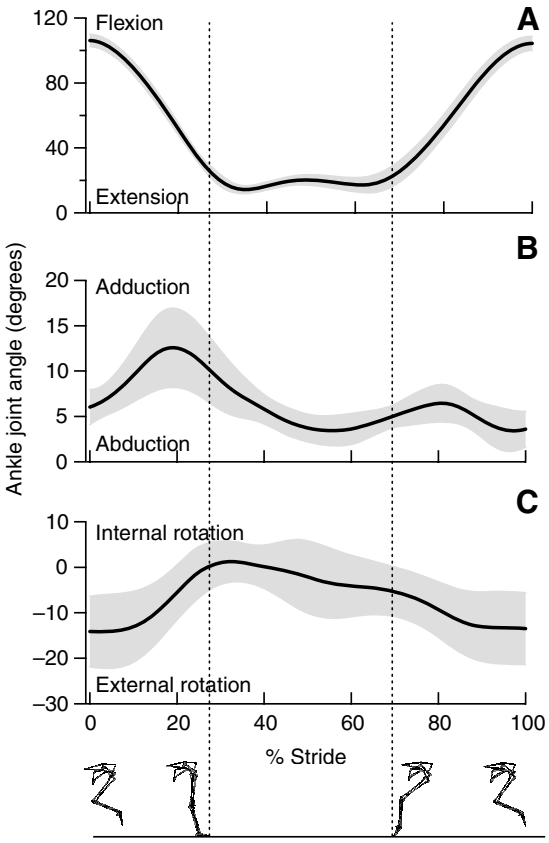

Fig. 9. Ankle joint (A) flexion/extension, (B) adduction/abduction and (C) internal/external rotation angles over one running stride (mean ± s.d.). Each stride begins and ends at mid-swing. The broken lines represent toe-strike and toe-off.

solely responsible for lowering the toes to the ground before the next stance phase.

Sagittal plane pelvic movements (pelvic pitch) are relatively small and have little influence over the hip flexion/extension angles. This pelvic pitch pattern is similar to that observed for guinea fowl, also a terrestrial species, albeit with larger fluctuations (Gatesy, 1999). Other bird species do not exhibit any clear pattern of pelvic pitch during running, e.g. quail (Reilly, 2000) and magpie (Verstappen et al., 2000), perhaps reflecting a difference in cursoriality. The mean pelvic pitch angle (12°) is considerably less than that of smaller bird species such as guinea fowl, quail and magpie (Gatesy, 1999; Reilly, 2000; Verstappen et al., 2000), although guinea fowl do exhibit similar pitch angles during fast running (Gatesy, 1999). The smaller pelvic pitch angle in ostriches supports the idea that large non-avian theropods (e.g. *Tyrannosaurus rex*) may have had a more horizontal sacral orientation compared to the earlier, more upright reconstructions [for a discussion on this topic see Gatesy (Gatesy, 1999)].

The overall pattern of knee flexion/extension over the running stride is similar to that of other bird species as well as that of human running. The majority of the knee flexion/extension occurs during the swing phase in the ostrich, whereby the knee contributes both to lifting the toes off the ground at the beginning of the swing phase and to returning the toes towards the ground for the initiation of the next stance phase. The knee has a similar pattern of flexion/extension during the swing phase in humans (Novacheck, 1998). In birds, however, knee flexion/extension appears somewhat more variable, with some studies on walking chicks reporting flexion followed by extension (Johnston and Bekoff, 1992; Johnston and Bekoff, 1996), while others report only knee extension during the swing phase in chicks (Muir et al., 1996), quail (Reilly, 2000) and magpie (Verstappen et al., 2000). The pattern of knee flexion followed by knee extension during stance has been observed in other smaller running birds (Gatesy, 1999; Verstappen et al., 2000) and humans (Novacheck, 1998), and may represent a strategy for storage and release of elastic energy and/or damping of the ground reaction force.

The ankle undergoes a large flexion/extension excursion during the swing phase and is the major joint responsible for repositioning the lower limb segments during swing. Other studies on chickens (Jacobsen and Hollyday, 1982), the silver gull (Dagg, 1977) and magpie (Verstappen et al., 2000) have likewise shown that flexion/extension at the ankle dominates the sagittal plane limb movements during the swing phase. Interestingly, however, the ankle remains static throughout most of the stance phase. The ankle joint has been regarded as a primary cite for elastic energy storage and return in running birds *via* the gastrocnemius tendon (e.g. Roberts et al., 1997). The lack of a flexion/extension movement at the ankle during stance in ostriches does not support this view, however, at least for the narrow range of speeds examined in this study. Interestingly, studies on chickens (Jacobsen and Hollyday, 1982; Johnston and Bekoff, 1992) and quail (Clark and Alexander, 1975) have also shown minimal flexion/extension during stance, indicating that spring-like behavior at the ankle should not be generalized to all birds over all running speeds.

The metatarso-phalangeal joint exhibits a very large

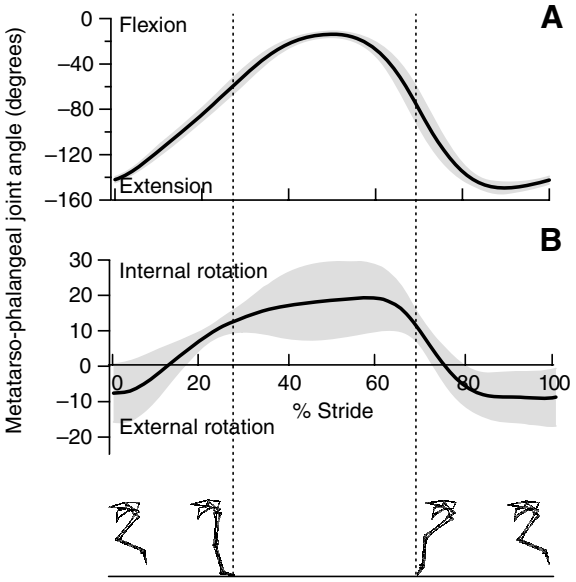

Fig. 10. Metatarso-phalangeal joint (A) flexion/extension and (B) internal/external rotation angles over one running stride (mean ± s.d.). Each stride begins and ends at mid-swing. The broken lines represent toe-strike and toe-off.

flexion/extension excursion, in particular during the swing phase. The flexion/extension observed during the stance phase likely contributes to storage/release of elastic strain energy in digital flexor tendons. These tendons are ideally suited for storage/release of elastic energy owing to their small cross sectional area and long length (~80 cm). It should be pointed out that the measured metatarso-phalangeal joint angle assumes a single phalanx segment and does not take into consideration movement at the inter-phalangeal joints. These joints likely undergo flexion/extension, especially during stance, and accurate measurements of muscle–tendon strain will benefit from their inclusion. For the purpose of this study a single segment is used to represent the overall movement of the phalanges. Interestingly, it is the metatarso-phalangeal joint rather than the ankle that likely provides the majority of the elastic energy storage/release *via* the digital flexor muscles (at least for the speeds examined in this study). In contrast, human bipedal running exhibits an ankle-based elastic storage/release system *via* the gastrocnemius muscles (Fukunaga et al., 2002; Lichtwark et al., 2007). Further examination of metatarso-phalangeal and ankle mechanics in other species will help reveal whether this represents a general difference in locomotor strategies between avian and human bipedalism.

The extent to which the metatarso-phalangeal joint excursion is actively mediated *via* muscle during the swing phase has been the topic of some discussion (Verstappen et al., 2000). Verstappen and colleagues raised the possibility that the bi-articular nature of the digital flexors and extensors (these also cross the ankle) may facilitate passive joint motion during the swing phase. However, while the action of the ankle may indeed transfer energy to move the phalanges *via* two-joint muscles, these muscles may need to be active to produce the required force, and would therefore still consume metabolic energy (although not producing any mechanical work). During the stance phase, where little ankle motion is present, strain in the muscle–tendon units crossing the metatarso-phalangeal joint are expected to primarily account for the movement of this joint.

Influence of flexion/extension axes alignment on 3-D kinematics

A critical feature of the ostrich knee and ankle joint anatomy that drastically influences the interpretation of 3-D segment motion is the alignment of their flexion/extension axes relative to the animal's direction of travel (relative to the sagittal plane). While the flexion/extension axis of the knee, and to a lesser extent the ankle, may shift throughout the joints' range of motion, the average helical axes are rotated externally to the direction of travel (see Fig. 5). This is evident not only from the average helical axes reconstructed from the anatomical modeling, but from helical axes calculated directly from the running trials (although these axes exhibit greater variability compared to those reconstructed from the anatomical specimens). As a result, pure flexion and extension at the knee will act to adduct and abduct the tibiotarsus relative to the plane of movement, and pure flexion and extension at the ankle will act to abduct and adduct the tarsometatarsus relative to the plane of movement.

Knowledge of the axis alignment of the joints is thus clearly important for interpreting locomotor kinematics and understanding how segment motion is controlled. In 2-D planar analyses it is often assumed that the flexion/extension axes of the joints lie perpendicular to the sagittal plane. In this situation, segment motion in the frontal plane may be erroneously interpreted as adduction/abduction at the level of the joint, or alternatively, what has been measured as joint flexion/extension in a sagittal plane analysis may actually incorporate rotation about non-flexion/extension axes (Gard et al., 1996). In 3-D analyses, joint kinematics are often based on joint axes constructed from anatomical landmarks (Cappozzo et al., 1995; Wu et al., 2002). For instance, many studies define the flexion/extension axis of the human knee from the medial and lateral femoral condyles (e.g. Cappozzo, 1995; Lucchetti et al., 1998). However, the actual flexion/extension axes can differ from these anatomical axes. As in 2-D analyses, misalignment of the flexion/extension axes results in kinematic cross-talk, where rotation about one axis is interpreted as rotation about another. In 3-D studies of human locomotion substantial kinematic cross-talk has been observed at the hip, knee and ankle depending on the alignment of flexion/extension axes (Kadaba et al., 1990; Piazza and Cavanagh, 2000; Marin et al., 2003; Besier et al., 2003). In the ostrich the average helical axes of the knee and ankle differ substantially from the assumed axes of rotation based on the medial and lateral borders of the joints (the medial and lateral femoral condyles and the medial and lateral base of the tarsometatarsus, respectively). Although we did not specifically quantify the degree of kinematic cross-talk that would result from using axes based on these anatomical landmarks, it is clear that this approach would substantially affect the rotations about all three axes at these joints.

In light of these observations the non-sagittal limb movements observed in the ostrich result, in large part, from flexion/extension at the level of the joint. Most notable is the motion of the tarsometatarsus during the swing phase. Because the ankle's flexion/extension axis is rotated externally relative to the sagittal plane (partly due to the orientation of the knee's flexion/extension axis that rotates the tibia externally), when the ankle flexes after toe-off the tarsometatarsus is abducted away from the body. This abduction is considerably larger than that of human running, as can be seen by a lateral displacement of the phalanx marker of 20 cm from toe-off to mid-swing. The segment is subsequently adducted back towards the body's centerline with ankle extension during the second half of the swing phase. Non-sagittal displacement of the tarsometatarsus is, therefore, not the result of adduction/abduction at the level of the joint, but rather due to the orientation of the ankle joint flexion/extension axis.

These 3-D features of the joint kinematics may also exist in other avian species. In an anatomical study of pigeon, a diagonal orientation of the knee's articulating surfaces that resulted in substantial 'lateral–medial swing' (abduction/adduction of the tibiotarsus) was described (Cracraft, 1971). This non-sagittal motion in the pigeon tibiotarsus thus appears to occur as a result of a rotated knee flexion/extension axis (relative to the sagittal plane). Furthermore, similar non-sagittal limb movements to those of the ostrich have been observed in running guineafowl; the tibiotarsus and tarsometatarsus have been reported to adduct relative to the animal's line of travel during stance and the tarsometatarsus exhibits an abduction–adduction pattern during

swing (Gatesy, 1999). It is possible that these segment motions also result from the alignment of the flexion/extension axis of their knee and ankle. At least in the ostrich, this characteristic of the joint anatomy appears to provide the major lateral displacement of the lower limb necessary for steering the swinging limb clear of the stance limb and may be a general feature of the avian limb.

Non-flexion/extension kinematics

Although the majority of joint motion in the ostrich occurs about the joint flexion/extension axes, it is evident that 3-D segment motion in this species depends also on rotations about the joints' adduction/abduction and internal/external rotation axes. For instance, hip abduction and adduction during the stance phase has similar magnitude to the joint flexion/extension range of motion, and during the swing phase the hip exhibits a similar magnitude of abduction as flexion. This may reflect an equal requirement of this joint to provide the lateral displacement of the limb and to swing the limb forward. Interestingly, abduction at the hip will increase the degree of external rotation of the ankle flexion/extension axis by rotating the entire limb about the cranial axis (due to the horizontal posture of the femur). This results in greater abduction of the lower limb that is coupled to ankle flexion.

The requirement for hip abduction during the swing phase may stem in part from the minimal pelvic yaw that could otherwise aid in abducting the limb segments and provide clearance between the swing and stance limbs. In this regard, it is interesting to note that the magnitude of hip abduction is similar to that observed for guineafowl (Gatesy, 1999), a species that also exhibits little pelvic yaw when running. Other 'waddling' species (e.g. ducks, penguins) exhibit considerable pelvic yaw and roll, in part to position the body center of mass over the stance foot. Further studies incorporating 3-D joint kinematics are required to reveal whether waddling bird species also exhibit substantial joint adduction/abduction to provide limb clearance and balance, or whether limb adduction/abduction and waddling represent two distinct strategies for avian bipedal locomotion.

Throughout the stride the femur is in an externally rotated orientation relative to the pelvis. However, the results from this study suggest that little internal/external rotation occurs at the hip, although some internal rotation may exist during late stance and the early part of the swing phase. It is important to note, however, that the hip internal/external rotation exhibited large variability between the animals and between separate trials of the same animal, possibly reflecting limitations in the measurement techniques. The calculation of long-axis femur rotation assumed that the external femur marker cluster represented the underlying limb movement. Because the markers cannot easily be secured around the thigh segment on ostriches, some long-axis rotation may occur underneath the marker cluster. More accurate calculation of femoral rotation in this species may require cineradiography techniques or the use of bone pins secured directly to the femur.

The magnitude of the knee's varus/valgus and internal/external range of motion are similar to studies on human locomotion (Lafortune et al., 1992). The knee exhibits a surprisingly similar varus/valgus pattern to that found in human walking, whereby the knee undergoes a valgus–varus excursion both during the stance phase and during the swing phase (Besier et al., 2003), albeit with a slightly greater range of motion compared to humans. During human running, however, the knee has been found to undergo a small valgus–varus–valgus excursion during stance (Ferber et al., 2003). Given the bow-legged frontal plane limb posture in ostriches, the increase in the valgus joint angle during stance was unexpected, since it is likely that the forces at the knee tend to adduct it at this time. The magnitude of knee internal/external rotation is only moderately greater in ostriches compared to humans, although during stance the ostrich knee rotates externally, compared to the internal rotation found in humans. During swing, external rotation followed by internal rotation is evident in both humans and ostriches.

Given that valgus and external tibial rotation were coupled to knee flexion, and that varus and internal tibial rotation were coupled to knee extension in the unloaded ostrich knee, it is possible that similar coupling occurs during running as a result of joint architecture and ligamentous constraints at the knee. Interestingly, similar coupled motions have been reported in the ostrich and pigeon knee joint (Cracraft, 1971; Fuss, 1996), and are thought to be controlled by ligamentous constraints and the shape of the meniscus-fibular and condyle surfaces (Cracraft, 1971; Fuss and Gasser, 1992; Fuss, 1996). It should be noted that the internal tibiotarsus rotation, coupled with external femur rotation during knee flexion reported in Fuss (Fuss, 1996), is represented by valgus rotation in the present study due to the definition of the knee joint coordinate system. These coupled motions are commonly referred to as 'screw-home' motion and are also a characteristic feature of the human knee joint (Markolf et al., 1976; Wilson et al., 2000). The magnitude of the varus/valgus and internal/external motion was, however, considerably greater in running ostriches compared to the *in situ* analyses, suggesting that the joint path could be exaggerated under load. It is also possible that the coupled joint motions observed at the knee are, in part, the result of kinematic cross-talk. Using functionally derived axes, such as those applied in this study, should minimize kinematic cross-talk (Besier et al., 2003). However, when the flexion/extension axis of rotation shifts throughout the joint range of motion, the average flexion/extension axis is not representative of the true axis at all joint angles and kinematic cross-talk may result. Whether the observed non-flexion/extension motion observed at the knee during running should be regarded as true varus/valgus and internal/external rotation, or whether it is the result of a rotating flexion–extension axis is therefore debatable. In the latter case, little or no varus/valgus and internal/external rotation outside of the knee's 'neutral' position would have been calculated over the range of flexion/extension angles, although the rotation of the axis would itself cause the tibiotarsus to rotate substantially within the current joint coordinate system axes. Finally, it should not be ruled out that errors in varus/valgus rotation at the knee propagate from errors in calculating internal/external rotation of the femur.

Although the three-dimensional kinematics of the knee joint are complex and not fully understood, there are aspects that can be viewed in a functional context. In this regard it is perhaps easier to interpret the swing phase of running. Here, external

rotation and valgus motion during the early and middle part of the swing phase, respectively, aid in abducting the lower limb segments away from the centerline, thereby improving the clearance between the swing and stance limb. Subsequently, the large varus motion and internal rotation during the end of the swing phase contributes to returning the phalanges underneath the body prior to toe-strike.

The lack of substantial ankle adduction/abduction and internal/external rotation during the stance phase is consistent with the view that the ankle in birds is a simple hinge joint (Clark and Alexander, 1975) and also reflects the static nature of the ankle joint during stance. However, during swing the ankle exhibits moderate non-flexion/extension rotations. These rotations seem unlikely, given the traditional notion of the ankle as a hinge joint and since the unloaded joint excursion indicates that external rotation is coupled to ankle flexion rather than ankle extension. Ankle joint kinematics may be different under load, when the joint compressive force and muscle moments have an influence. In this case, the function of the adduction and long-axis rotation of the tarsometatarsus at the end of swing may align the phalanges in the plane of movement prior to toe-strike, a motion that may be required given that the tarsometatarsus is itself not aligned in this plane. The notion that considerable non-flexion/extension motions occurs at the avian ankle joint is also supported by a study on pigeon (Cracraft, 1971), where as much as 50° internal/external rotation and 15° abduction/adduction were reported to exist in anatomical specimens.

The non-flexion/extension rotation at the ankle may also be due to systematic measurement error. Although no such error is obvious, kinematic cross-talk or systematic movement of the tarsometatarsus marker cluster may play a role. The prominent internal/external rotation of the metatarso-phalangeal joint during the end of stance and through the swing phase was also unexpected, considering this joint is also primarily a hinge joint. This result may be due to the placement of the phalanx marker that did not completely isolate movement of the inter-phalangeal joints, and thus any lateral displacement of the phalanges could influence the internal/external rotation angle. It is also possible that the calculated flexion/extension axis differed slightly from the true axis, resulting in kinematic cross-talk.

Implications for avian bipedal biomechanics

The current study adopted techniques developed in 3-D human gait analysis in the study of avian bipedal gait. Amongst the most central findings arising from this study is the discrepancy between the alignment of the joint axes of rotation assumed in 2-D analyses (parallel with frontal plane) and those calculated in 3-D. This observation not only influences measurements of 3-D joint kinematics and interpretation of 3-D segment motion, but has important implications for other aspects of avian bipedal biomechanics. For instance, axis misalignment has the potential to alter calculations of net joint moments and muscle moment arms about joint axes, which can lead to subsequent errors in calculating joint mechanical power or when decomposing net joint moments into lumped muscle forces or individual muscle forces using optimization modeling. These errors would be expected to alter conclusions regarding the motor control of locomotion as well as conclusions regarding mechanical/muscular efficiency and the metabolic cost of producing muscle force. Further work is required to address this issue.

The current study shows how these potential errors can be minimized in 3-D analyses of locomotor biomechanics in birds. Although the reconstructions of the ACSs depend on relatively simple geometric scaling between the live animal and anatomical specimens, the modeling techniques used here provide greater accuracy than more simple identification of joint centers and axes; the errors in predicting the joint center locations between two anatomical specimens were within 15 mm in nearly all the TACS axes and approach the digitizing error of the kinematic data acquisition used in the running trials. Similar anatomical modeling can be applied to other bipedal species using suitable anatomical landmark data, or by combining methods described in the present study with x-ray data, or alternatively, the sacrifice of the experimental animal for validation of landmark location may be desired. For small species, the methods outlined can be adopted in x-ray cinematography to provide superior identification of the skeletal features used in constructing the kinematic model.

Finally, our results illustrate that locomotion in avian bipeds is a complex, 3-D task requiring coordination of more than just flexion/extension of the joints. A good example of this level of complexity is seen during the swing phase, where abduction at the hip, varus/valgus and internal/external rotation at the knee and flexion/extension at the ankle may all contribute to abducting the swing limb away from the stance limb and repositioning the phalanges under the body prior to the next toe-strike. Interestingly, the alignment of the ankle flexion/extension axis in birds may replace what would otherwise require adduction/abduction and/or internal/external rotation, allowing for a less complex joint, musculoskeletal geometry and neuromuscular control. These findings may provide valuable clues into the relationships between avian bipedal musculoskeletal structure and function, and its evolution.

Appendix

Definition of segment technical anatomical coordinate systems (TACSs)

The technical anatomical coordinate systems are right-handed Cartesian coordinate systems that are defined from palpable anatomical landmarks and projected landmarks. Importantly, the TACSs are not used to define the joint motion, but rather allow reconstruction of the anatomical coordinate systems (ACS). The definitions of the TACSs are listed below (for definitions of the landmark abbreviations see Table A1).

Pelvis: same as pelvis ACS (see below)

Femur:
- origin: LFC
- *y*-axis: unit vector from TROCH C. and LFC (positive being proximal)
- *z*-axis: cross product of *y*-axis and unit vector from HJC and TROCH C. (positive being lateral)
- *x*-axis: cross product of *y*-axis and *z*-axis

Tibiotarsus:
- origin: Mid.TROCH
- *y*-axis: unit vector from KJC and Mid.TROCH (positive being proximal)
- *z*-axis: cross product of *y*-axis and unit vector

Table A1. *Definitions of anatomical landmarks and numerically derived landmarks*

	Definition
Anatomical landmarks	
Pelvis	
IL	Cranial aspect of the ilium, where it meets the sixth thoracic vertebrae.
SUL	Sulcus: caudal end of the prominent ridge on the midline of the dorsal aspect of the postacetabular ilium
SYN	The caudal end of the synsacrum where it meets the first tail vertebra
PUB	Caudal end of pubis (alternative point for construction of a pelvis anatomical coordinate system)
Femur	
TROCH C.	Trochanteric crest
LFC	Lateral femoral condyle
Tibiotarsus	
L.TROCH	Lateral tibial trochlea (also referred to as condyle)
M.TROCH	Medial tibial trochlea (also referred to as condyle)
Tarsometatarsus	
LMB	Lateral metatarsal base
MMB	Medial metatarsal base
LMH	Lateral metatarsal head
MMH	Medial metatarsal head
Phalanges	
PHAL	Distal end of phalanx III
Derived landmarks	
HJC	Hip joint center
KJC	Knee joint center
LKHA	Lateral knee helical axis endpoint
MKHA	Medial knee helical axis endpoint
AJC	Ankle joint center
LAHA	Lateral ankle helical axis endpoint
MAHA	Medial ankle helical axis endpoint
Mid.TROCH	Midpoint between L.TROCH and M.TROCH
TJC	Toe joint center (metatarso-phalangeal joint center)
LTHA	Lateral toe helical axis endpoint
MTHA	Medial toe helical axis endpoint
Mid.MB	Midpoint between LMB and MMB
Mid.MH	Midpoint between LMH and MMH

Table A2. *Location of anatomical landmarks and numerically derived landmarks in the technical anatomical coordinate systems (TACSs) as a percent of segment scaling factors*

Point	Relative segment coordinate system	Endpoints used for scaling	Length (m)	Location in coordinate system (%)		
				x	*y*	*z*
HJC	*Pelvis TACS	IL–SYN	0.5130	–34.54	–6.19	10.12
HJC	*Pelvis TACS	IL–SUL	0.2687	–65.94	–11.81	19.31
KJC	Femur TACS	TROCH C.–LFC	0.2623	5.86	0.06	17.03
LKHA	Femur TACS	TROCH C.–LFC	0.2623	45.07	–6.49	–4.48
MKHA	Femur TACS	TROCH C.–LFC	0.2623	–2.91	16.61	21.84
AJC	Tibia TACS	KJC–Mid.TROCH	0.5011	5.21	–0.68	–1.14
AJC	Tibia TACS	L.TROCH–M.TROCH	0.0724	36.02	–4.72	–7.85
LAHA	Tibia TACS	KJC–Mid.TROCH	0.5011	7.54	1.81	–21.39
LAHA	Tibia TACS	L.TROCH–M.TROCH	0.0724	52.16	12.52	–147.92
MAHA	Tibia TACS	KJC–Mid.TROCH	0.5011	4.78	–1.14	2.58
MAHA	Tibia TACS	L.TROCH–M.TROCH	0.0724	33.06	–7.89	17.87
TJC	Tarsometatarsus TACS	Mid.MB –Mid.MH	0.4372	–2.72	4.87	–0.70
TJC	Tarsometatarsus TACS	LMH –MMH	0.0552	–21.57	38.55	–5.56
LTHA	Tarsometatarsus TACS	Mid.MB –Mid.MH	0.4372	–0.67	3.17	–20.42
LTHA	Tarsometatarsus TACS	LMH –MMH	0.0552	–5.36	25.07	–161.8
MTHA	Tarsometatarsus TACS	Mid.MB –Mid.MH	0.4372	–3.74	5.72	9.15
MTHA	Tarsometatarsus TACS	LMH –MMH	0.0552	–29.67	45.28	72.46

*Note: the pelvis TACS is its ACS (anatomical coordinate system). For other abbreviations, see Table A1.

from M.TROCH and L.TROCH (positive being lateral)
x-axis: cross product of *y*-axis and *z*-axis

Tarsometatarsus origin: Mid.MB
y-axis: unit vector from Mid.TROCH and Mid.MB (positive being proximal)
z-axis: cross product of *y*-axis and unit vector from MMH and LMH (positive being lateral)
x-axis: cross product of *y*-axis and *z*-axis

Phalanges not required.

Definition of segment anatomical coordinate systems (ACSs) and joint motion

The segment anatomical coordinate systems are right-handed Cartesian coordinate systems defined either from palpable anatomical landmarks (pelvis) or the joint centers and joint flexion/extension helical axes (femur, tibiotarsus, tarsometatarsus and phalanges). The joint centers and helical axes are located from their position within the TACSs, expressed relative to their scaling factors (see Table A2). The definitions of the ACSs are listed below (for definitions of the landmark abbreviations, see Table A1).

Pelvis origin: IL
x-axis: unit vector from SUL and SYN (positive being anterior)
y-axis: cross product of *x*-axis and unit vector from IL and SUL (positive being cranial)
z-axis: cross product of *x*-axis and *y*-axis

Femur origin: KJC
z-axis: unit vector from MKHA and LKHA (positive being lateral)
y-axis: cross product of *z*-axis and unit vector from HJC and KJC (positive being proximal)
x-axis: cross product of *y*-axis and *z*-axis

Tibiotarsus origin: AJC
y-axis: unit vector from KJC and AJC (positive being proximal)
z-axis: cross product of *y*-axis and unit vector from MAHA and LAHA (positive being lateral)
x-axis: cross product of *y*-axis and *z*-axis

Tarsometatarsus origin: TJC
y-axis: unit vector from AJC and TJC (positive being proximal)
z-axis: cross product of *y*-axis and unit vector from MTHA and LTHA (positive being lateral)
x-axis: cross product of *y*-axis and *z*-axis

Phalanges origin: TJC
x-axis: unit vector from TJC and PHAL (positive being anterior)
z-axis: cross product of *x*-axis and unit vector from MTHA and LTHA (positive being lateral)
y-axis: cross product of *x*-axis and *z*-axis.

Reconstruction sequence for the anatomical coordinate systems

The anatomical coordinate systems on the live animal were reconstructed from a series of spatial transformations based on the anatomical landmark data collected during the static calibration trials. First, the pelvis anatomical landmarks were used to define the pelvis/trunk ACS, and with the use of each bird's pelvic scaling factors the location of the HJC was estimated. After the HJC was transposed into the femur TCS, the femur TACS and scaling factor could be defined, from which the femur ACS could be reconstructed, which included the knee joint center (KJC) and the knee helical flexion/extension axis. After this, the KJC from the femur ACS was transposed into the tibiotarsus TCS so that the tibia TACS and scaling factor could be defined, from which the tibia ACS was reconstructed. A transformation matrix of the femur's ACS relative to the tibiotarsus TACS allowed the KJC to be located from both the femur and tibiotarsus TACS. The tarsometatarsus TACS and scaling factor were defined directly from the ALs located with the pointer, allowing reconstruction of the tarsometatarsus ACS. Finally, the phalanges ACS was constructed from the ALs of the tarsometatarsus and the phalanx marker. These spatial transformations made it possible to reconstruct each segment ACS from the motion data of the segment marker clusters across running strides.

The authors are grateful to the Heliams family for kindly providing the location for the over-ground running experiments and thank Daina Sturnieks, Mano, Steven Mulls and Shane Maloney for their assistance in data collection. The authors also wish to thank two anonymous reviewers for their valuable comments and criticisms. Russell Main provided the image used in Fig. 1. This project was supported by an Australian Research Council grant to P.A.F. and D.G.L.

References

Abourachid, A. and Renous, S. (2001). Bipedal locomotion in ratites (Paleognatiform): examples of cursorial birds. *Ibis* **142**, 538-549.
Besier, T. F., Sturnieks, D. L., Alderson, J. A. and Lloyd, D. G. (2003). Repeatability of gait data using a functional hip joint centre and a mean helical knee axis. *J. Biomech.* **36**, 1159-1168.
Biewener, A. A. (2002). Future directions for the analysis of musculoskeletal design and locomotor performance. *J. Morphol.* **252**, 38-51.
Cappozzo, A. (1984). Gait analysis methodology. *Hum. Mov. Sci.* **3**, 27-54.
Cappozzo, A., Catani, F., Della Croce, F. and Leardini, A. (1995). Position and orientation in space of bones during movement: anatomical frame definition and determination. *Clin. Biomech.* **10**, 171-178.
Clark, J. and Alexander, R. M. (1975). Mechanics of running by quail (*Coturnix*). *J. Zool. Lond.* **176**, 87-113.
Cracraft, J. (1971). The functional morphology of the hind limb of the domestic pigeon, *Columba livia*. *Bull. Am. Nat. Hist.* **144**, 171-268.
Dagg, A. L. (1977). The walk of the silver gull (*Larus novaehollandiae*) and of other birds. *J. Zool. Lond.* **182**, 529-540.
Fedak, M. A., Heglund, N. C. and Taylor, C. R. (1982). Energetics and mechanics of terrestrial locomotion. II. Kinetic energy changes of the limbs and body as a function of speed and body size in birds and mammals. *J. Exp. Biol.* **97**, 23-40.
Ferber, R., Davis, I. M. and Williams, D. S., 3rd (2003). Gender differences in lower extremity mechanics during running. *Clin. Biomech.* **18**, 350-357.
Fukunaga, T., Kawakami, Y., Kubu, K. and Kanehisa, H. (2002). Muscle and tendon interaction during human movements. *Exerc. Sports. Sci. Rev.* **30**, 106-110.
Fuss, F. K. (1996). Tibiofibular junction of the South African ostrich (*Struthio camelus australis*). *J. Morphol.* **227**, 213-226.
Fuss, F. K. and Gasser, C. R. (1992). Cruciate ligaments of the avian knee: insights into a complex system. *J. Morphol.* **214**, 139-151.
Gard, S. A., Knox, E. H. and Childress, D. S. (1996). Two-dimensional representation of three-dimensional pelvic motion during walking: an example of how projections can be misleading. *J. Biomech.* **29**, 1387-1391.
Gatesy, S. M. (1991). Hind limb movements of the American alligator (*Alligator mississippiensis*) and postural grades. *J. Zool. Lond.* **224**, 577-588.
Gatesy, S. M. (1999). Guineafowl hind limb function. I: Cineradiographic analysis and speed effects. *J. Morphol.* **240**, 115-125.
Gatesy, S. M. and Biewener, A. A. (1991). Bipedal locomotion: effects of

speed, size and limb posture in birds and humans. *J. Zool. Lond.* **224**, 127-147.

Grood, E. S. and Suntay, W. J. (1983). A joint coordinate system for the clinical description of three-dimensional motions: application to the knee. *J. Biomech. Eng.* **105**, 136-144.

Hutchinson, J. R. (2004). Biomechanical modeling and sensitivity analysis of bipedal running ability. II. Extinct taxa. *J. Morphol.* **262**, 441-461.

Hutchinson, J. R. and Gatesy, S. M. (2000). Adductors, abductors, and the evolution of archosaur locomotion. *Paleobiology* **26**, 734-751.

Irschick, D. J. and Jayne, B. C. (1999). Comparative three-dimensional kinematics of the hindlimb for high-speed bipedal and quadrupedal locomotion of lizards. *J. Exp. Biol.* **202**, 1047-1065.

Jacobsen, R. D. and Hollyday, M. (1982). A behavioral and electromyographic study of walking in the chick. *J. Neurophysiol.* **48**, 238-256.

Jayne, B. C. and Irschick, D. J. (1999). Effects of incline and speed on three-dimensional hindlimb kinematics of a generalized iguanian lizard (*Dipsosaurus dorsalis*). *J. Exp. Biol.* **202**, 143-159.

Johnston, R. M. and Bekoff, A. (1992). Constrained and flexible features of rhythmical hindlimb movements in chicks: kinematic profiles of walking, swimming and airstepping. *J. Exp. Biol.* **171**, 43-66.

Johnston, R. M. and Bekoff, A. (1996). Patterns of muscle activity during different behaviors in chicks: implications for neural control. *J. Comp. Physiol. A* **179**, 169-184.

Kadaba, M. P., Ramakrishnan, H. K. and Wootten, M. E. (1990). Measurement of lower extremity kinematics during level walking. *J. Orthop. Res.* **8**, 383-392.

Lafortune, M. A., Cavanagh, P. R., Sommer, H. J., 3rd and Kalenak, A. (1992). Three-dimensional kinematics of the human knee during walking. *J. Biomech.* **25**, 347-357.

Leardini, A., Cappozzo, A., Catani, F., Toksvig-Larsen, S., Petitto, A., Sforza, V., Cassanelli, G. and Giannini, S. (1999). Validation of a functional method for the estimation of hip joint center of location. *J. Biomech.* **32**, 99-103.

Lichtwark, G. A., Bougoulias, K. and Wilson, A. M. (2007). Muscle fascicle and series elastic element length changes along the length of the human gastrocnemius during walking and running. *J. Biomech.* **40**, 157-164.

Lucchetti, L., Cappozzo, A., Cappello, A. and Della Croce, U. (1998). Skin movement artefact assesment and compensation in the estimation of knee joint kinematics. *J. Biomech.* **31**, 977-984.

Marin, F., Mannel, H., Claes, L. and Durselen, L. (2003). Correction of axis misalignment in the analysis of knee rotations. *Hum. Mov. Sci.* **22**, 285-296.

Markolf, K. L., Mensch, J. S. and Amstutz, H. C. (1976). Stiffness and laxity of the knee: the contributions of the supporting structures. A quantitative in vitro study. *J. Bone Joint Surg. Am.* **58**, 583-594.

Most, E., Axe, J., Rubash, H. and Li, G. (2004). Sensitivity of the knee joint kinematics calculation to selection of flexion axes. *J. Biomech.* **37**, 1743-1748.

Muir, G. D., Gosline, J. M. and Steeves, J. D. (1996). Ontogeny of bipedal locomotion: walking and running in the chick. *J. Physiol.* **493**, 589-601.

Novacheck, T. F. (1998). The biomechanics of running. *Gait Posture* **7**, 77-95.

Piazza, S. J. and Cavanagh, P. R. (2000). Measurement of the screw-home motion of the knee is sensitive to errors in axis alignment. *J. Biomech.* **33**, 1029-1034.

Piazza, S. J., Erdemir, A., Okita, N. and Cavanagh, P. R. (2004). Assessment of the functional method of hip joint center location subject to reduced range of hip motion. *J. Biomech.* **37**, 349-356.

Reilly, S. M. (2000). Locomotion in the quail (*Coturnix japonica*): the kinematics of walking and increasing speed. *J. Morphol.* **243**, 173-185.

Reilly, S. M. and Elias, J. A. (1998). Locomotion in *Alligator mississippiensis*: kinematic effects of speed and posture and their relavance to the sprawling-to-erect paradigm. *J. Exp. Biol.* **201**, 2559-2574.

Reinschmidt, C. and van den Bogert, A. J. (1997). *KineMat: a MATLAB Toolbox for Three-dimensional Kinematic Analysis*. Calgary: Human Performance Laboratory, University of Calgary.

Roberts, T. J. and Scales, J. A. (2004). Adjusting muscle function to demand: joint work during acceleration in wild turkeys. *J. Exp. Biol.* **207**, 4165-4174.

Roberts, T. J., Marsh, R. L., Weyand, P. G. and Taylor, C. R. (1997). Muscular force in running turkeys: the economy of minimizing work. *Science* **275**, 1113-1115.

Roberts, T. J., Chen, M. S. and Taylor, C. R. (1998). Energetics of bipedal running. II. Limb design and running mechanics. *J. Exp. Biol.* **201**, 2753-2762.

Rubenson, J., Heliams, D. B., Lloyd, D. G. and Fournier, P. A. (2004). Gait selection in the ostrich: mechanical and metabolic characteristics of walking and running with and without an aerial phase. *Proc. R. Soc. Lond. B Biol. Sci.* **271**, 1091-1099.

Spoor, C. W. and Veldpaus, F. E. (1980). Rigid body motion calculated from spatial co-ordinates of markers. *J. Biomech.* **13**, 391-393.

Verstappen, M. and Aerts, P. (2000). Terrestrial locomotion in the black-billed magpie. I. Spatio-temporal gait characteristics. *Motor Control* **4**, 150-164.

Verstappen, M., Aerts, P. and Van Damme, R. (2000). Terrestrial locomotion in the black-billed magpie: kinematic analysis of walking, running and out-of-phase hopping. *J. Exp. Biol.* **203**, 2159-2170.

Whittle, M. W. (1995). Musculoskeletal applications of three-dimensional analysis. In *Three-dimensional Analysis of Human Movement* (ed. P. Allard, I. A. F. Stokes and J. Blanchi), pp. 295-310. Champaigne, IL: Human Kinetics.

Wilson, D. R., Feikes, J. D., Zavatsky, A. B. and O'Connor, J. J. (2000). The components of passive knee movement are coupled to flexion angle. *J. Biomech.* **33**, 465-473.

Wu, G. and Cavanagh, P. R. (1995). ISB recommendations for standardization in the reporting of kinematic data. *J. Biomech.* **28**, 1257-1261.

Wu, G., Siegler, S., Allard, P., Kirtley, C., Leardini, A., Rosenbaum, D., Whittle, M., D'Lima, D. D., Cristofolini, L., Witte, H. et al. (2002). ISB recomendation on definitions of joint coordinate system of various joints for the reporting of human joint motion – part I: ankle, hip, spine. *J. Biomech.* **35**, 543-548.